Crystal Structure of Tetragonal and Monoclinic Polytypes of Tschernichite, the Natural Counterpart of Synthetic Zeolite Beta

A. Alberti,[†] G. Cruciani,[†] E. Galli,[‡] S. Merlino,[§] R. Millini,[||] S. Quartieri,[‡] G. Vezzalini,[‡] and S. Zanardi*,[†]

Dipartimento di Scienze della Terra, Università di Ferrara, I-44100 Ferrara, Italy, Dipartimento di Scienze della Terra, Università di Modena, I-41100 Modena, Italy, Dipartimento di Scienze della Terra, Università di Pisa, I-56100 Pisa, Italy, and EniTecnologie S.p.A., Via F. Maritano 26, I-20097 San Donato Milanese, Milano, Italy

Received: May 16, 2002; In Final Form: July 23, 2002

The tetragonal and monoclinic polytypes of tschernichite (the natural counterpart of zeolite beta) from Mt. Adamson (Antarctica) were isolated and studied by single-crystal X-ray diffraction using a diffractometer equipped with a CCD detector. Diffraction patterns were interpreted with the help of the OD theory, and synthetic precession images allowed us to overcome ambiguities regarding the symmetry assignment. The two crystalline phases isolated are characterized as two MDO polytypes, tetragonal and monoclinic with different crystal sizes (small and large crystals, respectively), morphologies (single tetragonal dipyramids and radiating hemispherical groups, respectively), and chemistries (high and low Si/Al ratio, respectively). Both refined structures showed regular T−O distances (in the range 1.56−1.68 Å), and extraframework ions spreading over a large number of sites with low occupancy. Many independent sites were identified in both polytypes: in the monoclinic type three sites are occupied by Ca, whereas in the tetragonal three are occupied by Ca and one by Mg. The location and coordination of the site with the highest Ca occupancy in the monoclinic polytype were satisfactorily reproduced by potential energy calculations.

Introduction

Zeolite beta is a large-pore, high-silica aluminosilicate, first synthesized by Wadlinger et al.[1] using tetraethylammonium (TEA) as a structure directing agent. Its peculiar pore structure and acidity make zeolite beta one of the most important acid catalysts for several reactions including alkylation,[2,3] acylation,[4,5] disproportionation, and transalkylation[6,7] of aromatics, as well as alkylation,[8,9] cracking,[10] and isomerization[11,12] of paraffins, etc. Due to its outstanding performances, zeolite beta is presently employed in the EniChem industrial process for the alkylation of benzene with propylene to produce cumene.[13]

The crystal structure of zeolite beta was resolved in 1988 by Newsam et al.[14] using primarily high-resolution electron microscopy, electron diffraction, computer-assisted modeling, and powder X-ray diffraction and by Higgins et al.[15] through "a combination of model building, distance-least-squares refinement and powder pattern simulation". According to Newsam et al.[14] "zeolite beta can be regarded as a highly intergrown hybrid of two distinct, but closely related structures", whereas Higgins et al.[15] describe zeolite beta as a disordered structure consisting of "three ordered polytype structures", two of which correspond to the two polytypes proposed by Newsam et al.[14] Marler et al.[16] in an X-ray single crystal study on a hydrothermally synthesized zeolite beta, pointed out that this material can be described as an OD (order−disorder) structure built up by equivalent layers; in those structures (Dornberger-Schiff[17]) neighboring layers can be arranged in two or more geometrically, and therefore energetically, equivalent ways; distinct ways of stacking neighboring layers allow the existence of a series of both disordered and ordered (polytypes) sequences, all of them constituting one family of OD structures.

In 1993 Boggs et al.[18] described a new natural zeolite (found at Goble, Columbia County, Oregon) named tschernichite and showed that this material is the natural counterpart of zeolite beta. A new occurrence of tschernichite was recently reported at Mt. Adamson, Northern Victoria Land, Antarctica.[19]

The aim of this work is to study the structural features of tschernichite from Mt. Adamson and to compare them with those of synthetic zeolite beta.

Occurrence, Morphology, and Chemistry

Mt. Adamson, Northern Victoria Land, has been the site of very extensive Mesozoic-to-recent magmatic activity. The area is characterized by a crystalline basement (Paleozoic granites) overlain by a 35 m thick layer of sandstone (Bacon sediments), capped by about 450 m of basalt rocks (Ferrar dolerites).[20] Tschernichite has been found in fractures of basalts and grows over a thin layer of Fe-rich smectite. The mineral occurs either as large, steep tetragonal dipyramids up to 0.6 × 0.6 × 1.2 mm in size, terminating in a basal pinacoid, or as radiating hemispherical groups of small crystals (large and small drusy crystals were reported for Goble tschernichite too[18]). Crystals have slightly curved faces, with thin striae orthogonal to the dipyramid axis on their surfaces (see Figure 1). At high magnification, the edges of the pyramids are wavy and rough. Basal pinacoids show peculiar growth forms very similar to those found in synthetic beta (see Figure 2). The chemical composition was obtained by an electron microprobe operating

[†] Università di Ferrara.
[‡] Università di Modena.
[§] Università di Pisa.
[||] EniTecnologie S.p.A.

10.1021/jp021222h CCC: $22.00
Published on Web 09/10/2002

TABLE 1: Chemical Formulas of Tschernichite

	From Mt. Adamson (Antartica)	
large crystals	$Na_{1.6}K_{0.4}Mg_{0.4}Ca_{7.8}(Al_{17.8}\ Si_{46.2})O_{128}\cdot 67H_2O$	Si/Al = 2.6, Mg/Ca = 0.05
small crystals	$Na_{1.6}K_{0.4}Mg_{1.7}Ca_{3.8}(Al_{12.8}\ Si_{51.2})O_{128}\cdot 65H_2O$	Si/Al = 4.0, Mg/Ca = 0.45
small crystals	$Na_{1.6}K_{0.3}Mg_{3.5}Ca_{2.0}(Al_{12.8}\ Si_{51.2})O_{128}\cdot 65H_2O$	Si/Al = 4.0, Mg/Ca = 1.75
	From Goble (Oregon)[a]	
large crystals	$Na_{0.4}K_{0.0}Mg_{0.6}Ca_{7.7}(Al_{16.2}\ Si_{47.8})O_{128}\cdot 64H_2O$	Si/Al = 2.9, Mg/Ca = 0.08
small crystals	$Na_{0.9}K_{0.2}Mg_{0.0}Ca_{5.8}(Al_{13.4}\ Si_{50.6})O_{128}\cdot 64H_2O$	Si/Al = 3.8, Mg/Ca = 0.0

[a] Boggs et al.[18]

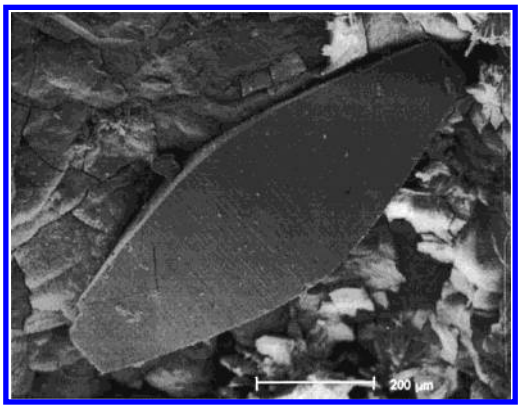

Figure 1. SEM image of a large dipyramidal crystal of tschernichite from Mt. Adamson.

at 15 kV, 20 nA, with a defocusing beam of 25 μm; the water content was determined by thermogravimetric analysis on large crystals. Table 1 reports the chemical formula of large and small crystals of tschernichite from Mt. Adamson. The chemical composition of large crystals was homogeneous both in Si/Al ratio and in extraframework cations, whereas in small crystals the Mg/Ca ratio varied remarkably in different crystals; Table 1 reports the chemical formulas of the crystals with the lowest and highest Mg/Ca ratio, respectively. It is to be noted that, whereas remarkable differences in this ratio were found in different crystals, the same crystal displayed a homogeneous composition; for comparison, the chemical formulas of Goble tschernichite are also reported. Table 1 clearly shows that large crystals are richer in Al than small ones, as applies also to tschernichite from Goble. The Mg content, however, seems to be far higher in small crystals than large ones: this does not appear in Goble tschernichite.

Structural Features

Higgins et al.[15] and Newsam et al.[14] were able to establish the lattice geometry of zeolite beta from electron and X-ray diffraction data, and to evidence an *hk*0 orthogonal net with $a = b \approx 12.5$ Å. These authors report the occurrence of sharp reflections at $h = 3n$ and $k = 3n$ in *h*0*l* and 0*kl*, respectively, and of diffuse streaks for $h \neq 3n$ and $k \neq 3n$, suggesting a disordered structure along *c** and indicating that the disorder is characterized by $\pm^1/_3 a$ and $\pm^1/_3 b$ displacements within the (001) plane. Both groups of authors agree that zeolite beta must be regarded as the disordered stacking of different polytypes. However, according to Newsam et al.,[14] zeolite beta can be described as a disordered sequence of only two polytypes, one tetragonal with symmetry $P4_122$ (or $P4_322$) and $a = b \approx 12.5$ Å and $c \approx 26.4$ Å (polytype A in Higgins et al.[15] and Newsam et al.[14]), the other monoclinic with symmetry $C2/c$ and $a \approx b \approx 12.5\sqrt{2}$ Å, $c \approx 14.4$ Å, and $\beta \approx 114°$ (polytype B in Higgins et al.[15] and Newsam et al.[14]); according to Higgins et al.,[15] in addition to these, a third polytype is present in zeolite beta with monoclinic symmetry, space group $P2$ (actually $P2/c$), with $a \approx b \approx 12.5$ Å, c ≈ 27.6 Å, and $\beta \approx 107°$ (polytype C).

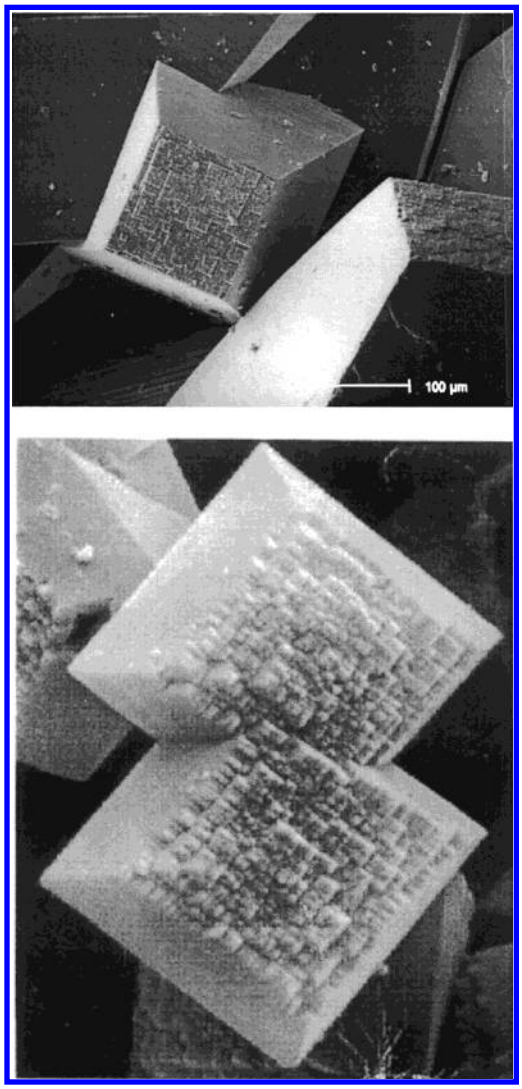

Figure 2. Growth forms on the smaller basal pinacoids of tschernichite from Mt. Adamson (top) and synthetic zeolite beta (bottom).

Smith et al.[21] in their study on tschernichite from Goble stated that the natural counterpart of zeolite beta consists of an intergrowth of A and B polytypes. This is in agreement with the study by Szostak et al.:[22] using high-resolution TEM images and electron diffraction patterns, these authors showed that tschernichite, as well as zeolite beta, is characterized by extremely high stacking fault frequencies. As pointed out by Galli et al.,[19] the powder pattern reported by Smith et al.[21] shows significant differences, mainly in the low θ range, from that reported for Mt. Adamson tschernichite; these differences in patterns may be attributed to a different ratio of the two A and B polymorphs and/or the presence of other beta-type polytypes.

This result will be exhaustively discussed later. However, the differences in chemistry associated with different morphologies observed for both Mt. Adamson and Goble tschernichite suggested that different structural features may differentiate these two types of crystals and encouraged us to try an X-ray single-crystal structure determination for both large and small crystals.

It seems fitting to recall that Newsam et al.,[14] besides the A and B polytypes, described another phase for zeolite beta, obtained by stacking successive layers without any displacement in the (001) plane. They denoted this phase as polymorph C, and it must be stressed that it differs from the C polytype described by Higgins et al.[15] Its cell parameters are $a = b \approx 12.5$ and $c \approx 13.3$ Å, space group $P4_2/mmc$, and its framework presents linear 12-membered-ring channels along *c*, as well as characteristic double 4-rings of tetrahedra. Newsam et al.[14] clearly stated that "neither electron diffraction micrographs, nor powder X-ray diffraction data provide any evidence for the occurrence of the structure C stacking arrangement in any of the zeolite beta samples studied" by them.

Very recently, preparations of the pure C structure-type or of distinct single-crystal pillars of the C structure-type overgrown on ordinary beta zeolite have been realized by Corma et al.[23] and Liu et al.,[24] respectively, from high Ge/Si and/or fluoride-containing media. Prior to this, Conradsson et al.,[25] from an aqueous solution containing germanium dioxide, pyridine, hydrofluoric acid, and 1,4-diazabicyclo[2,2,2]octane had obtained small needle-shaped crystals of $[(CH_3)_3N]_6[Ge_{32}O_{64}]\cdot(H_2O)_{4.5}$, tetragonal with $a = 22.990$, $c = 27.271$ Å, and space group $I4_1/amd$, characterized by a germanate framework displaying the same topology as structure-type C of Newsam et al.[14]

The neat distinction between this structure-type and the various polytypic forms of zeolite beta and tschernichite can be most clearly appreciated on the basis of the OD approach. The OD character of zeolite beta was first indicated by Marler et al.,[16] who prepared relatively large single crystals and collected the full set of sharp reflections, corresponding to the average structure (family structure in OD terminology), with $a = b = 4.121$, $c = 13.01$ Å, space group $P4_2/mmc$, and refined that substructure to conventional $R = 0.054$. The OD character has subsequently been briefly discussed by Böhme[26] and by Reinecke et al.[27] A more detailed presentation of the OD character of zeolite beta, and its natural counterpart tschernichite, will be presented elsewhere (Merlino et al. in preparation), together with indication of the correct symmetry properties of the whole family, descriptions of the most simple polytypes, and discussion of the two (not three, as maintained by Böhme) MDO structures, namely those sequences of OD layers realizing the maximum degree of order; in them, not only pairs but also triples, quadruples, and *n*-tuples of successive layers are geometrically equivalent. Here we focus attention on the crystal structure of tschernichite, pointing out that there is a correlation between polytypic form and chemical composition of the mineral.

Experimental Section

Intensity data were collected on a fragment of a large crystal and on a small crystal of tschernichite from Antarctica (dimensions of the crystals are reported in Table 2), using an automatic four-circle Nonius KappaCCD diffractometer equipped with a CCD detector (radiation MoKα). The package DENZO-SMN[28] was used for refinement of the unit cell and data reduction.

1. Large Crystals. Two sets of frames were collected:

(i) One set (10 frames), with a φ rotation width of 1° and an exposure time of 120 s per frame, was used for initial cell determination; a monoclinic unit cell with parameters comparable to those of the B polytype was immediately found.

(ii) A second set (total 90 images), with a φ rotation width of 2° and an exposure time of 4200 s per frame, was used for data collection. Refined cell parameters were $a = 17.983(3)$ Å, $b = 17.966(2)$ Å, $c = 14.625(2)$ Å, $\beta = 114.31(1)°$, and $V =$

TABLE 2: Data Collection, Unit Cell, and Refinement Parameters

diffractometer	Nonius KappaCCD	
radiation	MoKα	
crystal-to-detector distance	25 mm	
crystal	large crystal	small crystal
crystals dimensions	87 × 87 × 116 μm	58 × 58 × 87 μm
space group	*C*2/*c*	$P4_122$
cell parameters	$a = 17.983(3)$ Å	
	$b = 17.966(2)$ Å	$a = b = 12.634(1)$ Å
	$c = 14.625(2)$ Å	$c = 26.608(3)$ Å
	$\beta = 114.31(1)°$	
	$V = 4306$ Å^3	$V = 4247$ Å^3
maximum 2θ	55°	55°
no. of measured reflections	28 890	30 081
no. of unique reflections	4811	4879
no. of reflections used in the refinement with $F_o > 5\sigma(F_o)$	2604	1434
R_{int} %	17.9	21.3
final R_1[a]		
with $F_o > 5\sigma(F_o)$	0.129	0.106
no. of parameters	274	276
largest diffraction peak and hole	2.07; −0.84 e/Å^3	1.12; −0.80 e/Å^3

[a] $R_1 = \sum||F_o| - |F_c||/\sum|F_o|$.

TABLE 3: Atomic Coordinates, Occupancies, and Temperature Factors of Monoclinic Tschernichite

atom	*x*	*y*	*z*	occ	U_{eq}[a] or U_{iso}
T1	0.1708(3)	0.8334(3)	0.8880(4)	1.0	0.014(1)[a]
T2	0.2070(3)	0.5437(3)	0.1145(4)	1.0	0.017(2)[a]
T3	0.1924(3)	0.4185(3)	0.2512(4)	1.0	0.016(1)[a]
T4	0.3940(3)	0.0186(3)	0.6136(4)	1.0	0.018(1)[a]
T5	0.5201(3)	0.1450(2)	0.6140(4)	1.0	0.018(1)[a]
T6	0.5	0.2743(4)	0.75	1.0	0.014(1)[a]
T7	0.2971(3)	0.2926(2)	0.3892(4)	1.0	0.014(1)[a]
T8	0.4193(3)	0.1693(2)	0.3862(4)	1.0	0.016(1)[a]
T9	0.5	0.1116(4)	0.25	1.0	0.016(1)[a]
O1	0.2077(8)	0.9163(7)	0.8753(11)	1.0	0.032(3)[a]
O2	0.5784(8)	0.3306(8)	0.8014(10)	1.0	0.034(3)[a]
O3	0.2246(8)	0.7652(7)	0.8738(11)	1.0	0.033(3)[a]
O4	0.6681(8)	0.3329(7)	0.9996(9)	1.0	0.027(3)[a]
O5	0.2337(8)	0.4827(8)	0.2040(10)	1.0	0.032(3)[a]
O6	0.1451(8)	0.6024(8)	0.1324(12)	1.0	0.039(4)[a]
O7	0.1650(7)	0.5016(7)	0.0076(9)	1.0	0.026(3)[a]
O8	0.1672(9)	0.4554(9)	0.3359(10)	1.0	0.039(4)[a]
O9	0.2655(9)	0.3563(8)	0.3029(11)	1.0	0.041(4)[a]
O10	0.1153(8)	0.3825(9)	0.1592(10)	1.0	0.037(4)[a]
O11	0.4629(9)	0.0805(9)	0.6252(11)	1.0	0.047(4)[a]
O12	0.0637(9)	0.5621(9)	0.3419(11)	1.0	0.045(4)[a]
O13	0.5106(10)	0.2245(8)	0.6639(10)	1.0	0.041(4)[a]
O14	0.4987(7)	0.1623(7)	0.4944(8)	1.0	0.018(2)[a]
O15	0.3748(8)	0.2513(8)	0.3779(11)	1.0	0.032(3)[a]
O16	0.4506(8)	0.1689(8)	0.2959(10)	1.0	0.030(3)[a]
Ca1	0.1438(5)	0.3576(5)	0.0005(6)	0.52(2)	0.039(3)[a]
Ca2	0.305(3)	0.521(3)	−0.004(4)	0.073(8)	0.03(1)
Ca3	0.474(3)	0.696(3)	0.004(4)	0.079(9)	0.03(1)
W1	0.156(3)	0.224(3)	−0.114(4)	0.58(4)	0.12(2)
W2	0.118(3)	0.254(3)	−0.111(4)	0.45(4)	0.09(2)
W3	0.286(3)	0.347(3)	0.117(4)	0.41(4)	0.07(1)
W4	0.242(3)	0.378(3)	−0.108(3)	0.62(4)	0.11(1)
W5	0.396(3)	0.427(3)	0.126(3)	0.17(5)	0.18(8)
W6	0.478(5)	0.641(5)	−0.165(7)	0.26(4)	0.09(3)
W7	0.013(3)	0.140(3)	0.025(4)	0.56(4)	0.14(2)
W8	0.011(3)	0.021(3)	−0.019(3)	0.40(3)	0.04(1)
W9	0.145(3)	0.011(3)	0.007(4)	0.61(5)	0.14(2)
W10	0.091(3)	0.011(3)	0.194(5)	0.58(5)	0.14(3)

[a] $U_{eq} = (U_{11} + U_{22}\sin^2\beta + U_{33} + 2U_{13}\cos\beta)/[3(1 - \cos^2\beta)]$.

TABLE 4: Bond Distances (Å) and Percent of Al of Monoclinic Tschernichite

T1−O1	1.67(1)	T2−O1	1.64(1)
T1−O2	1.63(1)	T2−O5	1.62(1)
T1−O3	1.63(1)	T2−O6	1.64(1)
T1−O4	1.65(1)	T2−O7	1.62(1)
⟨T1−O⟩	1.64	⟨T2−O⟩	1.63
% Al	32	% Al	21
T3−O5	1.67(1)	T4−O7	1.68(1)
T3−O8	1.62(1)	T4−O8	1.63(2)
T3−O9	1.66(1)	T4−O11	1.62(2)
T3−O10	1.62(1)	T4−O12	1.64(2)
⟨T3−O⟩	1.64	⟨T4−O⟩	1.64
% Al	27	% Al	32
T5−O10	1.64(1)	T6−O2 (×2)	1.64(1)
T5−O11	1.61(1)	T6−O13 (×2)	1.62(1)
T5−O13	1.65(1)	⟨T6−O⟩	1.63
T5−O14	1.66(1)	% Al	22
⟨T5−O⟩	1.64	T8−O6	1.61(1)
% Al	27	T8−O14	1.64(1)
T7−O3	1.61(1)	T8−O15	1.66(1)
T7−O4	1.65(1)	T8−O16	1.64(1)
T7−O9	1.62(1)	⟨T8−O⟩	1.64
T7−O15	1.65(1)	% Al	26
⟨T7−O⟩	1.63	T9−O12 (×2)	1.63(1)
% Al	25	T9−O16 (×2)	1.67(1)
		⟨T9−O⟩	1.65
		% Al	31
		Ca2−O1	2.28(6)
		Ca2−O4	2.64(6)
Ca1−O7	2.61(2)	Ca2−O7	2.62(6)
Ca1−O10	2.61(2)	Ca2−O8	2.65(6)
Ca1−O12	2.61(2)	Ca2−W4	2.97(7)
Ca1−O14	2.60(2)	Ca2−W5	2.58(6)
Ca1−W1	2.87(5)	Ca3−O4	2.60(5)
Ca1−W2	2.38(5)	Ca3−O13	2.58(6)
Ca1−W3	2.44(5)	Ca3−O14	2.59(6)
Ca1−W4	2.85(5)	Ca3−O15	2.20(6)
		Ca3−W1	3.04(7)
		Ca3−W6	2.71(10)

4306.1 Å^3. Systematic extinctions were consistent with the *C*2/*c* space group.

The SHELX 93[29] least-squares computer program was used for structural refinement; this was carried out, according to the systematic extinctions, in the *C*2/*c* space group, starting from the DLS atomic coordinates of Higgins et al.[15] The structural refinement converged to a residual *R* value of 0.129 for 2604 unique reflections with $F_o > 5\sigma(F_o)$. Extraframework sites were located using F_o and ΔF Fourier maps.

Atomic coordinates, occupancy, and equivalent or isotropic temperature factors for the monoclinic zeolite tschernichite are reported in Table 3; bond distances and the Al fraction in tetrahedral sites are in Table 4.

2. Small Crystals. Five sets of frames were collected:

(i) The first set was used for cell determination (φ rotation width 1° and exposure time 180 s per frame); a tetragonal symmetry with cell parameters consistent with those of polytype A of Newsam et al.[14] was indicated.

(ii) One φ rotation (total 152 images) and three ω rotation sets (total 136 frames), with a rotation width of 1.2° and an exposure time of 1500 s per frame, were used for data collection.

Systematic extinctions were consistent with the $P4_122$ space group; the refined cell parameters were $a = b = 12.634(1)$ Å, $c = 26.608(3)$ Å, and $V = 4249.6$ Å^3. Structural refinement was carried out with the SHELX 93[29] computer program, starting from the DLS atomic coordinates of Higgins et al.[15] and converging to a residual *R* value of 0.106 for 1434 unique reflections with $F_o > 5\sigma(F_o)$. Extraframework sites were located using F_o and ΔF Fourier maps. It should be noted that the possible presence of both enantiomorphous structures ($P4_122$ and $P4_322$) does not affect the X-ray diffraction pattern. Atomic coordinates, occupancy, and equivalent or isotropic temperature factors for tetragonal tschernichite are reported in Table 5, and bond distances and Al fraction in tetrahedral sites are in Table 6.

TABLE 5: Atomic Coordinates, Occupancies, and Temperature Factors of Tetragonal Tschernichite

atom	*x*	*y*	*z*	occ	U_{eq}[a] or U_{iso}
T1	0.4579(5)	0.2945(5)	0.0562(2)	1.0	0.020(1)[a]
T2	0.4573(4)	0.0422(4)	0.0541(2)	1.0	0.018(1)[a]
T3	0.2111(4)	0.2935(4)	0.0565(2)	1.0	0.016(1)[a]
T4	0.2113(4)	0.0419(4)	0.0575(2)	1.0	0.017(1)[a]
T5	0.8360(5)	0.2938(4)	0.0566(2)	1.0	0.019(1)[a]
T6	0.8355(5)	0.0411(3)	0.0577(2)	1.0	0.018(1)[a]
T7	0.0271(3)	0.3583(4)	0.1251(2)	1.0	0.021(2)[a]
T8	0.0262(4)	−0.0262(4)	0.125	1.0	0.016(2)[a]
T9	0.6403(4)	0.3597(4)	0.125	1.0	0.019(2)[a]
O1	0.5	0.3395(19)	0.0	1.0	0.023(4)[a]
O2	0.4691(9)	0.1639(12)	0.0608(5)	1.0	0.035(4)[a]
O3	0.3363(10)	0.3310(13)	0.0631(4)	1.0	0.039(3)[a]
O4	0.5267(11)	0.3542(13)	0.0994(5)	1.0	0.037(4)[a]
O5	0.5	0.080(17)	0.0	1.0	0.030(4)[a]
O6	0.3340(12)	0.0018(12)	0.0626(4)	1.0	0.037(3)[a]
O7	0.5227(11)	−0.0180(12)	0.0993(5)	1.0	0.033(4)[a]
O8	0.2017(12)	0.1679(13)	0.0661(5)	1.0	0.047(5)[a]
O9	0.1643(10)	0.3224(14)	0.0018(4)	1.0	0.028(3)[a]
O10	0.1468(12)	0.3539(12)	0.1004(4)	1.0	0.036(4)[a]
O11	0.1641(14)	0.0056(16)	0.0024(3)	1.0	0.039(4)[a]
O12	0.1458(11)	−0.0208(12)	0.0998(4)	1.0	0.033(4)[a]
O13	0.8348(17)	0.1696(12)	0.0639(4)	1.0	0.050(3)[a]
O14	0.9374(12)	0.3480(12)	0.0809(4)	1.0	0.036(4)[a]
O15	0.7298(10)	0.3481(12)	0.0828(5)	1.0	0.057(5)[a]
O16	0.7296(11)	−0.0163(13)	0.0822(4)	1.0	0.035(4)[a]
O17	0.9412(11)	−0.0094(17)	0.0789(5)	1.0	0.050(5)[a]
Ca1	0.0	−0.123(3)	0.0	0.36(2)	0.11(1)
Ca2	0.0	0.449(2)	0.0	0.28(7)	0.05(7)
Ca3	−0.5	−0.318(4)	0.0	0.36(3)	0.10(1)
Mg	−0.295(5)	−0.307(5)	0.118(2)	0.08(3)	0.04(2)
W1	−0.186(5)	−0.229(3)	0.057(1)	0.55(5)	0.09(1)
W2	−0.167(4)	−0.416(3)	0.056(1)	0.93(5)	0.22(2)
W3	0.0	0.546(7)	0.0	0.38(5)	0.10(3)
W4	−0.359(4)	−0.206(4)	0.005(2)	0.86(5)	0.19(2)
W6	−0.463(5)	−0.323(6)	0.090(2)	0.67(5)	0.18(2)
W7	−0.361(6)	−0.478(6)	0.006(3)	0.31(5)	0.11(2)
W10	−0.155(4)	−0.346(6)	−0.002(2)	0.30(3)	0.06(1)
W11	−0.334(5)	−0.334(5)	−0.125	0.34(2)	0.08(2)
W13	0.0	−0.203(6)	0.0	0.38(3)	0.05(1)

[a] $U_{eq} = (U_{11} + U_{22} + U_{33})/3$.

Diffraction patterns of both tetragonal- and monoclinic-dominant crystals have in common a set of sharp reflections, with *h* (and *k*) = 3*n*, which are related to the family structure. Due to layer stacking disorder, diffuse peaks with *h* (and *k*) = $3n \pm 1$ are also present and are associated with continuous streaks elongated along *c**; the maxima distribution along these diffraction rows is characteristic for each stacking sequence (see Figure 3). Therefore, a detailed structural analysis of each polytype requires accurate intensity measurement of the diffuse peaks, which is typically hampered on serial goniometers; the 3-dimensional description of peaks, using an area-detector based diffractometer, allows a satisfactory integration of diffuse reflections. The pseudotetragonal diffraction pattern of all polytypes may give rise to possible ambiguities in the assessment of the real symmetry. For the two tschernichite crystals, these ambiguities were thoroughly checked with the help of synthetic precession images built up from the collected images.

Figure 3 shows tetragonal ($\bar{h}hl$) and (*hhl*) reciprocal lattice planes for both crystals. Intensity distributions along the [$\bar{5}5l$]

TABLE 6: Bond Distances (Å) and Percent of Al of Tetragonal Tschernichite

T1−O1	1.68(1)	T2−O2	1.56(2)
T1−O2	1.66(2)	T2−O5	1.60(1)
T1−O3	1.62(2)	T2−O6	1.65(2)
T1−O4	1.61(1)	T2−O7	1.64(1)
⟨T1−O⟩	1.64	⟨T2−O⟩	1.61
% Al	30	% Al	10
T3−O3	1.66(1)	T4−O6	1.64(2)
T3−O8	1.61(2)	T4−O8	1.61(2)
T3−O9	1.62(1)	T4−O11	1.65(1)
T3−O10	1.61(1)	T4−O12	1.61(1)
⟨T3−O⟩	1.63	⟨T4−O⟩	1.63
% Al	15	% Al	17
T5−O9	1.60(1)	T6−O11	1.66(1)
T5−O13	1.58(2)	T6−O13	1.63(2)
T5−O14	1.59(1)	T6−O16	1.66(1)
T5−O15	1.63(2)	T6−O17	1.59(2)
⟨T5−O⟩	1.60	⟨T6−O⟩	1.64
% Al	1	% Al	24
T7−O7	1.65(1)	T8−O12 (×2)	1.64(1)
T7−O10	1.65(1)	T8−O17 (×2)	1.65(1)
T7−O14	1.64(1)	⟨T8−O⟩	1.65
T7−O16	1.60(1)	% Al	29
⟨T7−O⟩	1.64	T9−O4 (×2)	1.62(1)
% Al	22	T9−O15 (×2)	1.61(1)
		⟨T9−O⟩	1.62
		% Al	7
Ca1−O11 (×2)	2.69(3)	Mg−O3	1.83(6)
Ca1−O17 (×2)	2.69(3)	Mg−O10	2.20(7)
Ca1−W1 (×2)	3.06(4)	Mg−W6	2.38(8)
		Mg−W1	2.44(8)
Ca2−O9 (×2)	2.68(2)	Ca3−W4 (×2)	2.26(6)
Ca2−O14 (×2)	2.68(2)	Ca3−W6 (×2)	2.47(6)
Ca2−W2 (×2)	3.05(5)	Ca3−W7 (×2)	2.73(9)

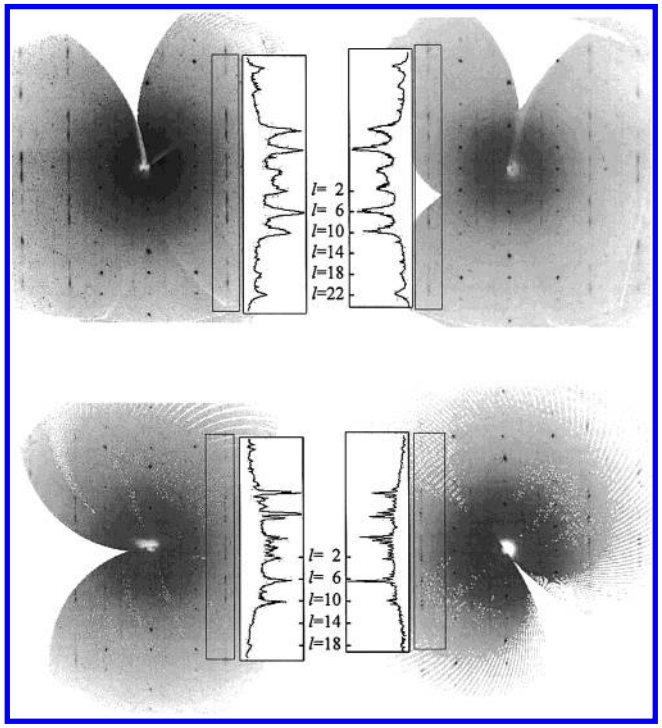

Figure 3. Precession images of tetragonal (above) and monoclinic (below) tschernichite crystals: ($\bar{h}hl$) reciprocal lattice planes on the left, and (hhl) reciprocal lattice planes on the right (tetragonal setting: $a \approx 12.6$, $c \approx 26.7$ Å). Intensity profiles along the [55l] (left) and [55l] (right) reciprocal lattice rows are also shown.

and [55l] diffraction rows are similar for the tetragonal-dominant crystal, as expected for a 4/m2/m2/m Laue group, whereas they differ remarkably for the monoclinic-dominant crystal, thus confirming the correct assignment of the two polytypes.

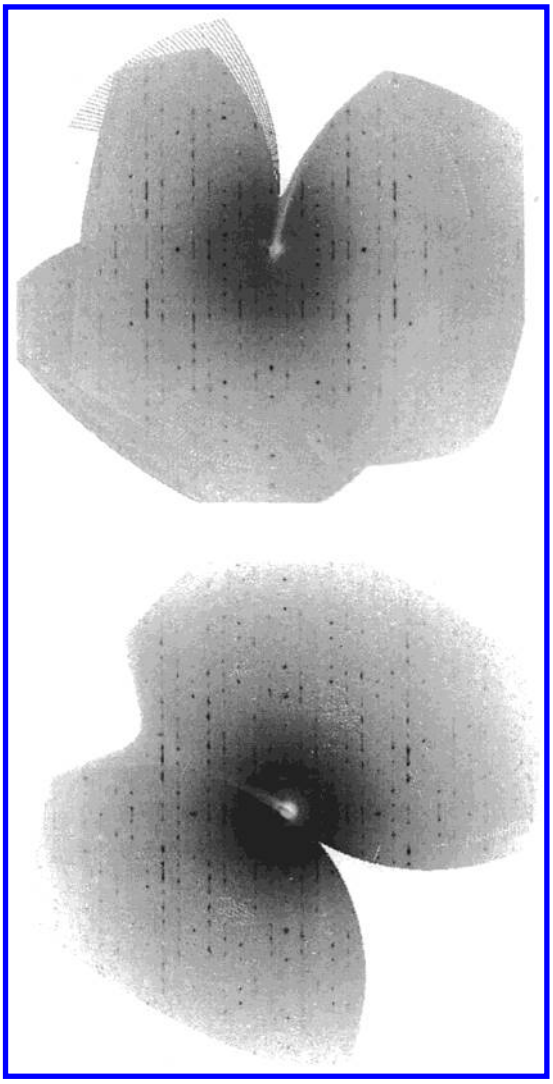

Figure 4. Precession images of the ($h0l$) reciprocal lattice planes of tetragonal (above) and monoclinic (below, tetragonal setting: $a \approx 12.6$, $c \approx 26.7$ Å) tschernichite crystals indicate that only very small amounts of other polytypic domains accompany the dominant polytype.

Moreover, a careful observation of ($h0l$) (indices refer to tetragonal cell) reciprocal lattice planes for both crystals (see Figure 4) clearly indicates that only very small amounts (if any) of other polytypic domains accompany the dominant polytype.

Computational Details

Ca^{2+} siting in the monoclinic polytype was determined using the Cation Locator algorithm from the Structure Solve module of the Cerius[2] software package.[30] The approach was that proposed by Gorman et al.,[31] which efficiently grids the interionic energies and populates the potential energy minima sites with extraframework cations. Calculations were performed on a purely siliceous model of the monoclinic polytype, corresponding to a 2 × 1 × 1 supercell with $P1$ symmetry. Two nonadjacent Si atoms of the distorted six-membered ring were substituted by Al, and a three-dimensional grid with 0.25 Å spacing was generated. The interionic interactions between Ca^{2+} and the framework were then computed at each point of the reference grid, using a 5.5 Å cutoff for short-range van der Waals interactions and Ewald summation[32] for long-range electrostatic interactions. Because the framework atoms were held still during the calculations, no valence energy terms were required. Calculations were carried out with the augmented

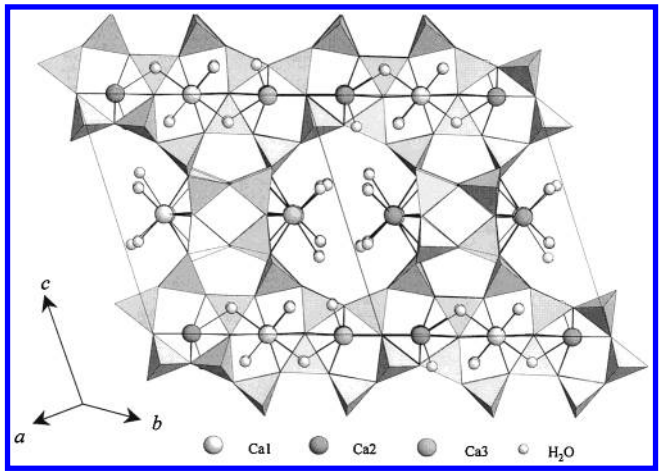

Figure 5. Polyhedral structure of the monoclinic dominant polytype of zeolite tschernichite. The coordinations of Ca sites are also shown.

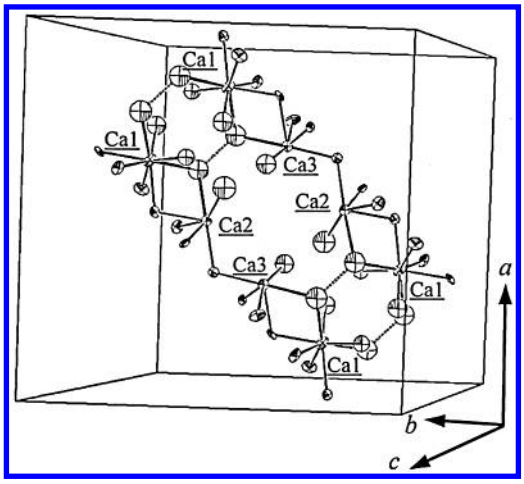

Figure 6. Chains of Ca-polyhedra along the (110) direction in the monoclinic polytype of tschernichite from Mt. Adamson.

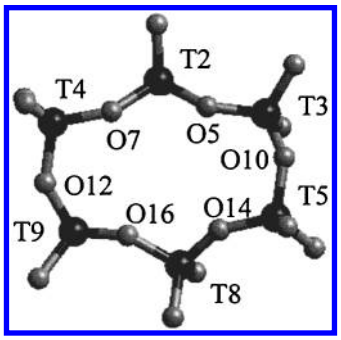

Figure 7. Distorted six-membered ring with the numbering scheme adopted.

cvff_aug force field (a modified *consistent valence force field* based on partial charges)[30] and included the experimentally determined position of water molecules. Almost all the extraframework water molecules were included in the calculations; only a few were excluded because they gave unrealistic O−O bonds when the model was built. This is a consequence of the impossibility to manage partial occupancy in the calculations. In the force field, the cations bore formal charges (2+ for Ca), whereas the following partial charges were assigned to the framework and water atoms: Si = +2.4, Al = +1.4, O = −1.2, H = +0.6. The final step of the calculation was geometry optimization of the models, performed with the Discover[33] program, using the COMPASS force field.[34] Even in this case, the framework and extraframework water molecules were held still at the crystallographically determined positions.

Results and Discussion

In accordance with the above discussion on tetragonal (*h*0*l*) synthetic precession images, in the following we shall refer to the large crystal where monoclinic polytype B (Newsam et al.[14] and Higgins et al.[15]) largely prevails as the "monoclinic polytype", and to the small crystal where tetragonal polytype A (Newsam et al.[14] and Higgins et al.[15]) largely prevails as the "tetragonal polytype".

Framework. Si/Al distribution is the most important crystal-chemical feature of the zeolite framework, affecting in particular its catalytic properties. Obviously no answer on this topic can be deduced by powder diffraction data, whereas reliable information could be obtained by a single-crystal-structure refinement.

The structural refinement of polytype *C*2/*c* shows a substantial disorder in the Si/Al distribution. According to Alberti and Gottardi's method,[35] the Al content in the tetrahedral sites varies in the range of 21−32% with an average value of 27%, in excellent agreement with the Al content found by the chemical analysis for large crystals (see Tables 1 and 4). Two straight 12-ring channels in the *C*2/*c* polymorph run parallel to [110] and [1$\bar{1}$0], respectively, and are connected through a 12-ring window. These channels are markedly elliptical, having minimum and maximum pore sizes of 6.9 and 7.5 Å for the channels parallel to [110] and [1$\bar{1}$0], respectively (see Figure 5), assuming a framework oxygen radius of 1.35 Å. It is to be noted that these values are quite similar to those obtained by Newsam et al.[14] by DLS refinement for polytype B. As concerns the 12-ring channel which "snakes" along *c*, its aperture dimensions are about 5.8 × 5.8 Å, slightly larger than those obtained by Newsam et al.[14]

Structural refinement of polytype $P4_122$ seems to indicate a more differentiated distribution of Al in tetrahedral sites. In fact, the Al content (calculated according to Alberti and Gottardi[35]) varies in the 1−30% range with an average content of 20%, in good agreement with the value of 17% given by chemical analysis. It must be pointed out that the high values of standard deviations on structural parameters suggest these results should be accepted with caution. The straight 12-ring channels, parallel in this polytype to the [100] and [010] directions, are strongly elliptic with a pore opening of 7.3 × 5.8 Å, whereas the tortuous 12-ring channel parallel to *c* has a pore size of about 5.8 × 5.8 Å, not far from the values found by Higgins et al.[15] and Newsam et al.[14]

Extraframework Sites. Three extraframework cation sites were found in the monoclinic polytype of tschernichite. These sites are distributed along the 12-ring channels parallel to the (001) plane, and form two chains of polyhedra on the opposite side of the channels. They all coordinate four framework oxygens (see Figure 5): one (Ca1 in Table 3), highly occupied, also coordinates four water molecules, whereas the other two (Ca2 and Ca3), weakly occupied, seem to coordinate only two water molecules. It is interesting to note that these cations form a chain, where one water molecule and one framework oxygen are shared by two adjacent calcium polyhedra (Figure 6).

Modeling studies were performed to verify the preferential Al siting through a comparison between the computed and the experimental Ca^{2+} location. Because of the high occupancy, only site Ca1, located slightly above the distorted six-membered ring (6MR, reported in Figure 7), was considered. Nine different models were built, each of them with two nonadjacent Si atoms

TABLE 7: Computed Fractional Coordinates for Ca^{2+} Sites and Distances from the Experimentally Determined Site

Al sites	*x*	*y*	*z*	$D_{calc-exp}$ (Å)
2−5	0.1417	0.3797	0.0336	0.639
2−8	0.1104	0.3560	−0.0146	0.549
2−9	0.1472	0.3819	−0.0183	0.533
3−4	0.1577	0.3905	0.0116	0.636
3−8	0.1173	0.3432	0.0094	0.602
3−9	0.1244	0.3616	−0.0157	0.339
4−5	0.1195	0.3733	−0.0003	0.516
4−8	0.1008	0.3644	−0.0375	0.754
5−9	0.1022	0.3502	−0.0212	0.695
exp	0.1438(5)	0.3576(5)	0.0005(6)	

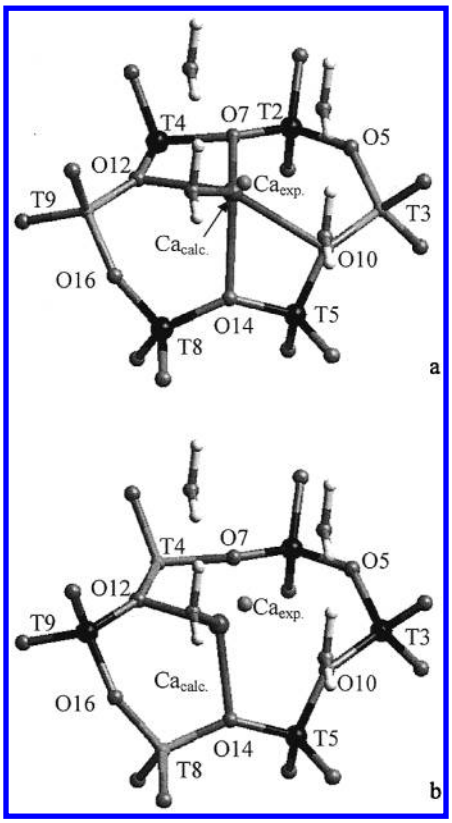

Figure 8. Location and bonding of Ca^{2+} ion upon substitution of Al in sites 3−9 (a) and 4−8 (b).

of the 6MR substituted by Al, and the corresponding Ca^{2+} positions were calculated. The fractional atomic coordinates for the cation sites for each of the models are listed in Table 7, together with the corresponding distance with respect to the experimentally determined position of site Ca1 ($D_{calc-exp}$). Inspection of these data revealed that the shortest $D_{calc-exp}$ value (0.339 Å) was computed for the model with Al atoms substituting Si3 and Si9, whereas significantly larger distances were computed for the other models ($D_{calc-exp}$ in the range 0.516−0.754 Å, Table 7). Figure 8 shows the coordination of Ca^{2+} in the most (3−9) and least (4−8) probable models. In the former, the Ca^{2+} ion is coordinated with four framework oxygens, the same oxygens (O_7, O_{10}, O_{12}, O_{14}) as found in the crystal structure refinement, with the Ca−O distance in the range 2.35−2.65 Å, in good agreement with the experimentally determined values (2−60 = 2.61 Å, Table 4). The same is true for the water molecules, with a Ca−W distance in the range 2.36−3.02 Å (Figure 8a). In the case of the 4−8 model, the coordination polyhedron of Ca^{2+} is characterized by short distances with two framework oxygens (2.08−2.13 Å) and with a water molecule (2.34 Å); consequently, all the other distances are very long, with the water molecules located at 3.12−3.23 Å (Figure 8b).

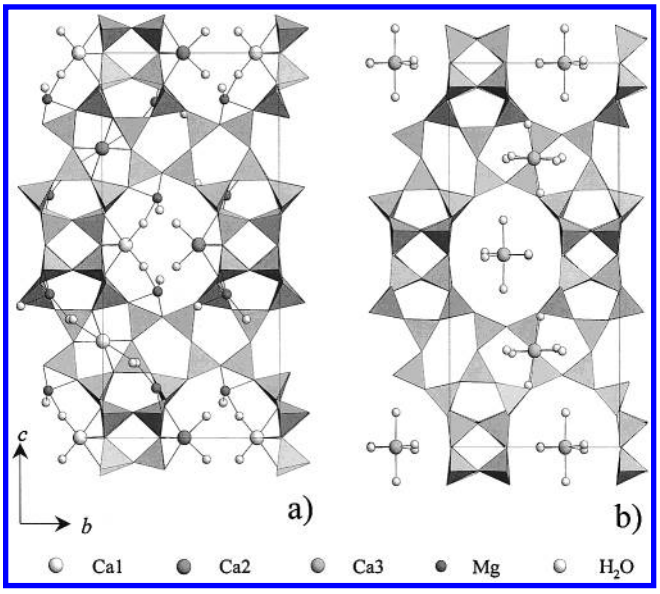

Figure 9. Polyhedral structure of the tetragonal dominant polytype of zeolite tschernichite. The coordinations of extraframework cations are also shown.

Concluding, the (3−9) model satisfactorily reproduces the experimental results.

It should be pointed out that water molecules of a chain have very short distances (2.4−2.6 Å) from water molecules of the chain on the opposite site of the channel, so that we cannot exclude the presence of strong hydrogen bonds between water molecules, among the strongest found in zeolites. Other partially occupied extraframework sites were located in the monoclinic polytype of tschernichite, which were attributed to water molecules. Two of these (W7 and W8 in Table 3) are near sites Ca2 and Ca3, so that Ca and W must be alternately present. The remaining water occupies the center of the 12-ring channels. Overall, the structural refinement affords 109 electrons for the extraframework cation sites and 309 electrons for water molecules, compared with the 177 and 534 electrons respectively afforded by the chemical analysis reported in Table 1.

In the tetragonal tschernichite polytype, four extraframework sites were attributed to cations; three of these (Ca1, Ca2, and Ca3 in Table 5) are occupied by Ca atoms (on the basis of their distances from framework oxygens and water molecules, and by analogy with the cation sites in polytype *C*2/*c*), the other by Mg (on the basis of its distances from framework oxygens). It is to be noted that Ca1 and Ca2 sites in tetragonal tschernichite occupy positions similar to the Ca1 site, the most occupied site in the monoclinic polytype (see Figure 9a). In the tetragonal phase the chain of Ca polyhedra exhibited by the monoclinic structure is not evident. However, the low Ca content in this polytype, together with the relatively low quality of the data, does not guarantee that such cation organization is absent in this phase. Both Ca1 and Ca2 sites are 6-coordinated with four framework oxygens and two H_2O molecules; the Ca3 cation is completely surrounded by water molecules, at the center of the channel system, in a near-perfect octahedral coordination (see Figure 9b), whereas Mg is coordinated by two framework oxygens and two H_2O molecules. As in the monoclinic structure, water molecules of polyhedra on the opposite side of the channels display short distances (≈ 2.4 Å), suggesting the possible presence of strong hydrogen bonds between water molecules. Many other partially occupied extraframework sites were found in the $P4_122$ phase. These were attributed to water molecules, because their large distances from framework

oxygens (2.7 Å) prevented us from having an unambiguous attribution of these sites to cations or water molecules, as is frequently found in the structural refinements of zeolites with wide channels and large cages. Overall, structural refinement affords 88 electrons for the extraframework cations and 312 electrons for the H_2O sites, compared with approximately 110 electrons for cations and 520 electrons for water molecules provided by the chemical analyses in Table 1.

It can be noted that the total number of electrons found in extraframework sites in both tschernichite polytypes is far lower than that given by chemical analysis (about 60% of the total). This result is, however, unsurprising, because many zeolites with strong disorder in the extraframework sites (as is the case of tschernichite) usually give a total electron number lower than the "true" one, as found for example in gottardiite[36] and mutinaite.[37]

Conclusions

Tschernichite-type zeolite found at Mt. Adamson showed that the two maximum degree of order (MDO) polytypes, in the sense of the order−disorder theory of Dornberger-Schiff,[17] constitute almost exclusively the building material of tschernichite and, by extension, the building material of zeolite beta. Moreover, this occurrence revealed the existence of natural phases displaying the structure-type of zeolite beta, with a large domain of one of the two MDO polytypes. The differences in chemistry seem responsible for the prevalence of either the monoclinic or tetragonal polytype and also give rise to distinct morphologies. The definition of these differences in chemistry and structure was made possible by the presence, in Mt. Adamson tschernichite, of crystals large enough for X-ray single-crystal-structure analysis. The discovery of this mineral's existence in nature is important also because we now know that

(i) an organic structure directing agent may not be necessary for synthesis, and

(ii) it is possible to obtain beta-type zeolite with an Si/Al ratio lower than that so far achieved in its synthetic counterpart.

It is noteworthy that almost all natural pentasil zeolites are present at Mt. Adamson: two of these [tschernichite and boggsite[19] (a mineral without synthetic counterpart)] have been found for the second time, whereas three [gottardiite[36] (the natural counterpart of synthetic NU-87), terranovaite[38] (a mineral without synthetic counterpart), and mutinaite[37] (the natural counterpart of synthetic ZSM-5)] have been found for the first time. It is evident that rather special conditions were involved in the crystallization of these zeolites, such as rapid cooling during crystal growth. If these conditions could be identified, a way to synthesis these phases (in particular the two different polytypes of beta zeolites) might be found.

A detailed study of the OD character of tschernichite to derive its main polytypes (MDO polytypes) and to define the structural features of the polytypic forms of tschernichite from Mt. Adamson is in progress (Merlino et al., manuscript in preparation).

Acknowledgment. We thank the Centro di Strutturistica Diffrattometrica of University of Ferrara for X-ray data collection. Italian CNR, PNRA, and MURST ("*Zeolites, materials of interest for industry and environment: synthesis, crystal structure, stability and applications*" and "*Structural complexity and mineral properties: microstructures, modularity, modulations*" COFIN 2001) are acknowledged for financial support. Special thanks to Dr. Francesco Di Renzo for SEM image of zeolite beta.

References and Notes

(1) Wadlinger, R. L.; Kerr, G. T.; Rosinski, E. J. U.S. Pat. 3 308069, 1967.

(2) Bellussi, G.; Pazzuconi, G.; Perego, C.; Girotti, G.; Terzoni, G. *J. Catal.* **1995**, *157*, 227.

(3) Perego, C.; Amarilli, S.; Millini, R.; Bellussi, G.; Girotti, G.; Terzoni, G. *Micropor. Mater.* **1996**, *6*, 395.

(4) Hoefnagel, A. J.; van Bekkum, H. *Appl. Catal. A* **1993**, *97*, 87.

(5) Kouwenhoven, H. W.; Gunnewegh, E. A.; van Bekkum, H. *Tagunsbericht* **1996**, *9601*, 9.

(6) Das, J.; Bath, Y. S.; Halgeri, A. B. *Catal. Lett.* **1994**, *23*, 161.

(7) Wang, I.; Tsai, T. C.; Huang, S. T. *Ind. Eng. Chem. Res.* **1990**, *29*, 2005.

(8) De Jong, K. P.; Mesters, C. M. A. M.; Peferoen, D. R. G.; van Brugge, P. T. M.; de Groot, C. *Chem. Eng. Sci.* **1996**, *51*, 2053.

(9) Nivarthy, G. S.; Feller, A.; Seshan, K.; Lercher, J. A. *Micropor. Mesopor. Mater.* **2000**, *35*−*36*, 75.

(10) Boretto, L.; Camblor, M. A.; Corma, A.; Perez-Pariente, J. *Appl. Catal.* **1992**, *82*, 37.

(11) Lee, J. K.; Rhee, H. K. *Catal Today* **1997**, *38*, 235.

(12) Wang, Z. B.; Kamo, A.; Youeda, T.; Komatsu, T.; Yashima, T. *Appl. Catal.* **1997**, *159*, 119.

(13) Perego, C.; Amarilli, S.; Bellussi, G.; Cappellazzo, O.; Girotti, G. *Proceedings of the 12th International Zeolite Conference*, Baltimore, MD, July 5−10, 1998; Treacy, M. M. J., Markus, B. K., Bisher, M. E., Higgins, J. B., Eds.; Materials Research Society: Warrandale, PA, 1999; p 575.

(14) Newsam, J. M.; Treacy, M. M. J.; Koetsier, W. T.; De Gruyter, C. B. *Proc. R. Soc. London, A* **1988**, *420*, 375.

(15) Higgins, J. B.; LaPierre, R. B.; Schlenker, J. L.; Rohrman, A. C.; Wood, J. D.; Kerr, G. T.; Rohrbaugh, W. J. *Zeolites* **1988**, *8*, 446.

(16) Marler, B.; Böhme, R.; Gies, H. In *Proceedings of the 9th International Zeolite Conference*, Montreal, 1992; von Ballmoos, R., Higgins, J. B., Treacy, M. M. J., Eds.; Butterworth-Heinemann: Stoneham, MA, 1993; p 425.

(17) Dornberger-Schiff, K. *Acta Crystallogr.* **1956**, *9*, 593.

(18) Boggs, R. C.; Howard, D. G.; Smith, J. V.; Klein, G. L. *Am. Mineral.* **1993**, *78*, 822.

(19) Galli, E.; Quartieri, S.; Vezzalini, G.; Alberti, A. *Eur. J. Mineral.* **1995**, *7*, 1029.

(20) Carmignani, L.; Ghezzo, C.; Gosso, G.; Lombardo, B.; Meccheri, M.; Montrasio, A.; Pertusati, P. C.; Salvini, F. *Mem. Soc. Geol. It.* **1987**, *33*, 77.

(21) Smith, J. V.; Pluth, J. J.; Boggs, R. C.; Howard, D. G. *J. Chem. Soc., Chem. Commun.* **1991**, 363.

(22) Szostak, R.; Pan, M.; Lillerud, K. P. *J. Phys. Chem.* **1995**, *99*, 91.

(23) Corma, A.; Navarro, M., T.; Rey F.; Rius, J.; Valencia, S. *Angew. Chem Int. Ed. Engl.* **2001**, *40*, 2277.

(24) Liu, Z.; Oshuna, T.; Terasaki, O.; Camblor, M, A., C.; Diaz-Cabañaz, M. J.; Hiraga, K. *J. Am. Chem. Soc*. **2001**, *123*, 5370.

(25) Conradsson, T.; Dadachov, M. S.; Zou, X. D. *Micropor. Mesopor. Mater.* **2000**, *41*, 183.

(26) Böhme, R. *Phase Transitions* **1993**, *43*, 95.

(27) Reinecke, K.; Steineke, U.; Jarchow, O.; Klaska, K.-H. Jahrstagung der Deutschen Gesellschaft für Kristallographie. *Z. Kristallogr.* **1999**, Suppl. Issue No. 16, 135.

(28) Otwinowski, Z.; Minor, W. *Methods Enzymol*. **1997**, *276*, 307.

(29) Sheldrick, G. M. SHELXL 1993, Program for crystal structure determinations. University of Cambridge, Cambridge, U.K., 1993.

(30) Cerius^2 Version 4.2 Materials Science. Molecular Simulations, Inc., San Diego, CA, 2000.

(31) Gorman, A. M.; Freeman, C. M.; Kölmel, C. M.; Newsam, J. M. *Faraday Discuss.* **1997**, *106*, 489.

(32) Ewald, P. P. *Ann. Phys.* **1921**, *64*, 253.

(33) Discover, force field simulations program. Molecular Simuations, Inc., San Diego, CA, 2000.

(34) Sun, H. *J. Phys. Chem. B* **1998**, *102*, 7338.

(35) Alberti, A.; Gottardi, G. *Z. Kristallogr.* **1988**, *184*, 49.

(36) Alberti, A.; Vezzalini, G.; Galli, E.; Quartieri, S. *Eur. J. Mineral.* **1996**, *8*, 69.

(37) Vezzalini, G.; Quartieri, S.; Galli, E.; Alberti, A.; Cruciani, G.; Kvick, Å. *Zeolites* **1997**, *19*, 323.

(38) Galli, E.; Quartieri, S.; Vezzalini, G.; Alberti, A.; Franzini, M. *Am. Mineral.* **1997a**, *82*, 423.